Onset of quenching of the giant dipole resonance at high excitation energies

D. Santonocito,[1] Y. Blumenfeld,[2] C. Agodi,[1] R. Alba,[1] G. Bellia,[1,3] R. Coniglione,[1] F. Delaunay,[2,*] A. Del Zoppo,[1]
P. Finocchiaro,[1] F. Hongmei,[1] V. Lima,[2] C. Maiolino,[1] E. Migneco,[1,3] P. Piattelli,[1] P. Sapienza,[1]
J. A. Scarpaci,[2,†] and O. Wieland[4]

[1]*INFN-Laboratorio Nazionale del Sud, Via S. Sofia 62, I-95123, Catania, Italy*
[2]*Institut de Physique Nucléaire, IN_2P_3-CNRS, F-91406 Orsay, France*
[3]*Dipartimento di Fisica e Astronomia dell'Universitá di Catania, Via S. Sofia 64, I-95123, Catania, Italy*
[4]*INFN - Sezione di Milano, Via Celoria 16, I-20133 Milano, Italy*

The evolution of the giant dipole resonance (GDR) properties in nuclei of mass $A = 120$ to 132 has been investigated in an excitation energy range between 150 and 270 MeV through the study of complete and nearly complete fusion reactions using ^{116}Sn beams at $17A$ and $23A$ MeV from the cyclotron of the Laboratorio Nazionale del Sud impinging on ^{12}C and ^{24}Mg targets. γ rays and light charged particles were detected using the multi-element detector array MEDEA in coincidence with evaporation residues detected by using mass and charge identification spectrometry with telescope (MACISTE). Light-charged-particle energy spectra were analyzed within the framework of a multiple-source-emission scenario by using a fitting procedure to determine the amount of pre-equilibrium emission and deduce the excitation energies reached in the compound nuclei. A detailed analysis of the γ-ray spectra and their comparison with statistical model calculations is presented. Evidence of a quenching of the GDR gamma yield was found at 270 MeV excitation energy. The quenching effect becomes progressively more important with increasing excitation energy, as observed when the comparison is extended to data from the reaction ^{36}Ar + ^{96}Mo at $37A$ MeV where hot nuclei were populated up to 430 MeV excitation energy. A coherent scenario emerges indicating the existence of a limiting excitation energy for the collective motion of about $E^*/A = 2.1$ MeV for systems of mass $A = 105$ to 111 while a slightly lower value was observed for nuclei of mass $A \sim 132$. The existence of a possible link between GDR disappearance and the liquid-gas phase transition is discussed.

PACS number(s): 24.30.Cz, 25.70.Gh, 25.70.Jj

I. INTRODUCTION

The isovector giant dipole resonance (GDR) has proven to be a valuable probe of the behavior of nuclei at high temperature, providing unique information on the bulk properties of the nucleus and on the evolution of collective motion at extreme conditions up to its disappearance [1]. While the main decay mode of the GDR is through light-particle emission, its γ decay branch is sufficiently large to probe its characteristics when it is built on highly excited compound nucleus states, which can be populated by complete or incomplete fusion reactions induced by heavy ions.

Many years of investigation have led to a comprehensive understanding of the evolution of the properties of the GDR with excitation energy or spin [2], the data being mainly collected for medium mass nuclei with $A \sim 110$ to 130. In this region the GDR centroid energy slightly varies between 14 and 15 MeV according to the $A^{-1/3}$ dependence [3] for $T = 0$ nuclei. With increasing excitation energy, below $E^* = 200$ MeV the centroid energy of the GDR may show a slight variation of few percent, the width increases due to temperature, spin effects and compound nucleus lifetime from 5 MeV up to about 14 MeV and the strength exhausts 100%

of the energy-weighted sum rule (EWSR) [4,5]. Above $E^* = 300$ MeV a suppression of the GDR γ emission was observed by several authors [6–8]. This is at variance with predictions of the statistical model from which a progressive increase of γ-ray multiplicity with excitation energy is expected due the higher number of steps available for the γ rays to compete with particle emission. To reproduce the data a sharp cutoff of the γ-ray emission above a certain excitation energy was introduced, pointing to a maximum excitation energy of approximately $E^*/A \sim 2.2$ MeV for which collective motion can be sustained in the nucleus [8]. This suppression of the GDR emission has been related to the equilibration time of the collective dipole vibration, which will become longer than the particle emission time above a certain limiting excitation energy. Several models have been put forward to reproduce the experimental behavior [9–13], but no precise understanding has been achieved, possibly because of lack of data in the excitation-energy region where the decrease of GDR emission sets in.

In order to fill this gap, a study of γ-ray emission from hot nuclei of mass $A \sim 120$ to 130 with excitation energies between 150 and 270 MeV was undertaken at the LNS Catania, using the Multi-Element Detector Array (MEDEA) [14] for γ rays and light-charged-particle detection. Since excitation-energy determination is crucial for an accurate understanding of the data, very asymmetric reactions giving rise to narrow excitation-energy distributions were chosen to populate hot nuclei through complete and incomplete fusion reactions.

———————
*Present address: Laboratoire de Physique Corpusculaire de CAEN, 14050 Caen Cedex, France.
†Present address: CSNSM-IN2P3-CNRS, F-91406 Orsay, France.

In particular, inverse kinematics reactions with ^{116}Sn beams impinging on ^{12}C and ^{24}Mg targets were used to take advantage of the large efficiency of the SOLE superconducting solenoid for residues emitted at small angles. Section II describes the experimental setup with a particular focus on the SOLE device and its detection system. In Sec. III the excitation energies attained in the different reactions will be evaluated through the measurement of the evaporation residues and the study of the light charged particles emitted. In Sec. IV the characteristics of the GDR deduced from the analysis of the γ-ray spectra will be given. Results from the analysis of a higher-energy experiment performed previously at the Grand Accelerateur National d'Ions Lourds (GANIL) will also be presented. In Sec. V the coherence of the results over a very large excitation-energy range will be demonstrated and discussed in light of predictions given by the statistical model. Evidence of a mass dependence of the limiting excitation energy for the collective motion and its possible link with a liquid-gas phase transition will be discussed in Sec. VI. A summary and outlook will be provided in Sec. VII.

II. EXPERIMENTAL METHOD

The experiment was carried out at the Laboratori Nazionali del Sud-Catania by using ^{116}Sn beams at $17A$ and $23A$ MeV with average intensities of 1.5 enA delivered by the Superconducting Cyclotron impinging on 1 mg/cm^2 ^{12}C and ^{24}Mg targets. Different projectile-target combinations, namely, ^{116}Sn + ^{12}C at $17A$ and $23A$ MeV, and ^{116}Sn + ^{24}Mg at $17A$ MeV, were used to populate hot nuclei through the mechanism of complete and incomplete fusion. Light charged particles and γ rays were detected in coincidence with evaporation residues by using the MEDEA + SOLE + MACISTE setup (see Fig. 1).

The MEDEA detector consists of a ball made of 180 BaF$_2$ scintillators, 20 cm thick and arranged in eight rings of 24 detectors covering the polar angles from 30° to 170° degrees and the whole azimuthal angle. Pulse shape analysis of the photomultiplier signal and time-of-flight information measured with respect to the cyclotron rf were used to identify γ rays and light charged particles. Details of the particle and γ-ray identification procedure and typical two-dimensional spectra can be found in Ref. [15]. The BaF$_2$ detectors were energy calibrated by using the 4.4 and 6.1 MeV γ rays emitted from AmBe and PuC sources. The calibration of

the light charged particles was deduced from the γ-ray one by using the procedure adopted in Ref. [16]. The suitability of the MEDEA scintillators for the measurement of γ rays stemming from the decay of the GDR has been largely demonstrated [17,18].

The fusion-like residues populated in the reactions and emerging from the target with polar angles below 3° were focused by the magnetic field of the superconducting solenoid SOLE on the focal plane detector MACISTE (mass and charge identification spectrometry with telescopes) placed 16 m from the target [19]. The superconducting solenoid SOLE is a forward collector for charged particles placed downstream the MEDEA scattering chamber (see Fig. 1). It covers $\simeq 40$ msr solid angle, has an angular acceptance of $\pm 6.5°$ which was reduced to 3° in this experiment due to the geometrical constraint related to the MULTICS apparatus (which was not used) and a momentum acceptance of $\pm 10\%$. A proper tuning of its magnetic field which can be set as high as 5 T allows for the optimization of the collection of the evaporation residues onto the focal place detector MACISTE while focusing noninteracting beam particles or elastically scattered ones through the central hole of the focal plane detectors. The focal plane detector MACISTE consists of four telescopes, 40×30 cm^2 each, arranged in a geometry resembling a photographic diaphragm leaving a variable central hole for beam transit [see Fig. 2(a)]. Each telescope consists of an ionization chamber for ΔE measurement, a low pressure multiwire proportional chamber (MWPC) for time-of-flight measurement and impact-point determination, and a plastic scintillator for E measurement. A schematic view is shown in Fig. 2(b). Each element of the telescope is divided in two parts in order to reduce pileup effects. The ionization chamber, 10 cm thick, operates with isobutane at a pressure ranging between 10 and 150 mbar, allowing for a variable effective thickness seen by the reaction products to be detected. It is divided in two regions with electric field perpendicular to the particle tracks and cathodes placed on both lateral surfaces of the detector. A Frisch grid is placed a few millimeters in front of the cathode plate in order to delimit the drift region of electrons towards the cathodes and remove any dependence of the induced signal on the distance from the electrode. The MWPC consists of two anodic planes made of 20 μm gold-plated tungsten wires separated by a double-sided aluminized mylar foil acting as a cathodic plane for both anodes [Fig. 2(b)]. The anode-cathode gap width is
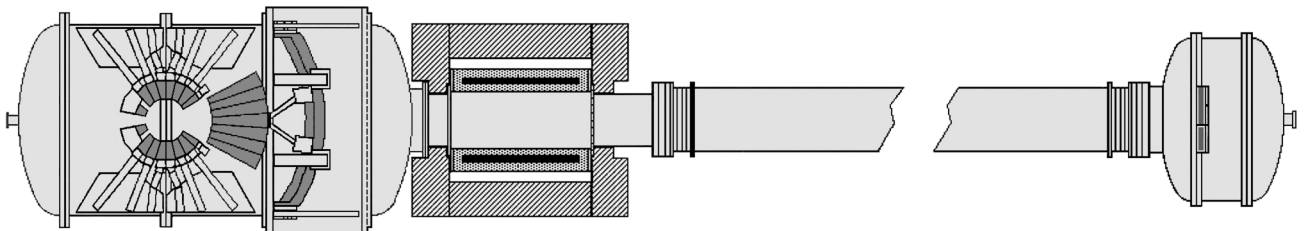
FIG. 1. Schematic drawing of the MEDEA - SOLE - MACISTE setup. The MEDEA multidetector is placed in the reaction chamber on the left and crystals are represented in dark gray. Adjacent to the MEDEA reaction chamber is placed the solenoid SOLE surrounding the beam line which allows to convey the reaction products to the focal plane detector MACISTE plotted in dark gray in the reaction chamber on the right end of the figure.
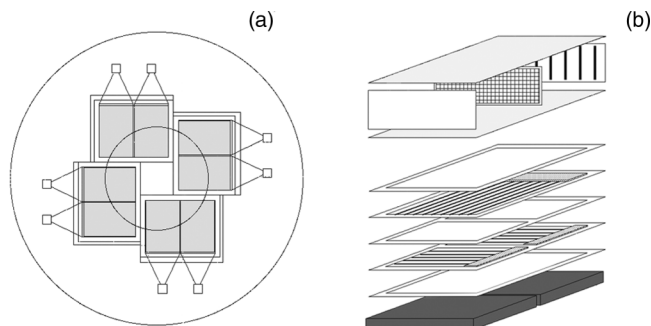
FIG. 2. (a) Front view of MACISTE detector consisting of four telescopes arranged in a variable geometry resembling a photographic diaphragm. A central hole is left for beam transit. The outer circle in the figure represents the size of the reaction chamber while the inner one shows the size of the beam line. Each telescope is divided in two parts. (b) Exploded view of a single telescope. From top to bottom are represented the ΔE ionization chamber separated in two parts, the MWPC with two anodic wire planes separated by a mylar foil, electrically split in two parts, acting as a cathodic plane and two outer mylar foils acting as entrance and exit windows and, in dark gray, the two plastic scintillators.

2 mm. The anodic wires are stretched, equally spaced in a step of 1 mm and glued onto an epoxy (stesalite) frame. One end of each wire is soldered to a printed circuit integrated onto a frame and a delay is placed between adjacent couples of wires. The charge collected on the wires and associated with the transit of a particle inside the detector is read at both ends of a delay chain and the time difference relative to a reference taken from the cathode is used to deduce the coordinates of the particle impact point. The longer side (40 cm length) is split into two equal parts and therefore two delay chains are used to read the electric signals. The MWPC operates at about 5 mbar isobutane pressure and allows one to determine the impact point with a resolution of about 3 mm in both coordinates and to measure the time of flight of the residues with an intrinsic resolution of about 500 ps. The E detector is a 2-cm-thick BC408 plastic scintillator. Its light readout is performed by a photomultiplier coupled to the detector through a light guide. Two plastic scintillators are used for each telescope.

For heavy residues such as those studied in the present experiment, unit mass and charge resolution is not obtained. Therefore, the major information extracted from MACISTE was the time of flight measured against the cyclotron rf. The time spectrum was calibrated by using a time calibrator and the offset was determined from the position of the elastic peak corrected for the energy loss in the target.

The trigger condition of the experiment was given by the coincidence between one multiwire chamber of MACISTE and at least one BaF$_2$ detector, with a threshold corresponding to approximately 2 MeV of γ-ray-deposited energy. The coincidence trigger limits the contamination of the γ-ray spectra due to the high-energy cosmic ray events to only random coincidences with heavy residues which, in the data analysis, were shown to be negligible. Runs with only MACISTE or MEDEA in trigger were also performed for calibration purposes.

III. EXCITATION-ENERGY DETERMINATION

The excitation energy of the states upon which the GDR is built is a crucial parameter for understanding the experimental results. At low incident energies it is generally assumed that complete fusion largely dominates the cross section for residue formation [20]. However pre-equilibrium emission has been shown to set in at beam energies as low as $5A$ to $7A$ MeV where, in mass-asymmetric systems, forward-focused α-particle emission has been observed, effectively lowering the excitation energy of the equilibrated compound system [21,22]. Above this beam-energy region, at about $10A$ MeV the more traditional incomplete fusion mechanism appears and becomes progressively more important with increasing beam energy [23,24]. Reactions where only part of the kinetic energy of the projectile is transferred to the composite system take place and pre-equilibrium light-particle and γ-ray emission is observed [25–27]. The analysis of the evaporation residue velocity distribution shows a centroid shifted to lower velocities, and a width which is, in general, broader than expected from complete fusion, revealing a sizable contribution of incomplete fusion events [23–25]. The broadening of the velocity distribution width reflects the contribution due the different momentum transfers leading to systems with different masses and excitations energies [15,25,28]. In this experiment very asymmetric systems were used for which the excitation-energy distribution is expected to be narrow which allows for a better determination of its value. This goal can be achieved through the measurement of the velocity of the evaporation residues and the analysis of the energy spectra of the light charged particles emitted in the reaction [17,18,26,28]. The time of flight of the residues was measured in order to characterize the mass transfer from target to projectile and the light-charged-particle spectra were analyzed to infer the energy removed by pre-equilibrium emission.

A. Time-of-flight spectra

The time of flight of the residues was measured with respect to the cyclotron rf to identify the fusion-like events. The spectra were calibrated by using a time calibrator and the position of the elastic peak which was extracted in a separate run where only the MACISTE detector was in trigger. The calibrated time-of-flight spectra for the three reactions are displayed in Fig. 3. A narrow peak corresponding to quasi-elastic scattering is visible in the spectra of Figs. 3(a) and 3(c) but absent in the spectrum of Fig. 3(b). In all three spectra the remainder of the distribution exhibits a maximum close to the center-of-mass velocity, indicating the presence of close-to-complete fusion events. The value of the maximum is consistent with a scenario of fusion of the projectile with the target during which pre-equilibrium particle emission takes place, lowering the excitation energies and mass of the composite system [26]. The width of the time-of-flight (ToF) distribution reflects the different linear momentum transfer contributions and the effect due to isotropic particle evaporation from the excited recoiling nucleus. The contribution of the time resolution ($\simeq1.5$ ns) and different transport lengths between target and detector is negligible. The reaction on the ^{24}Mg target displays a broader
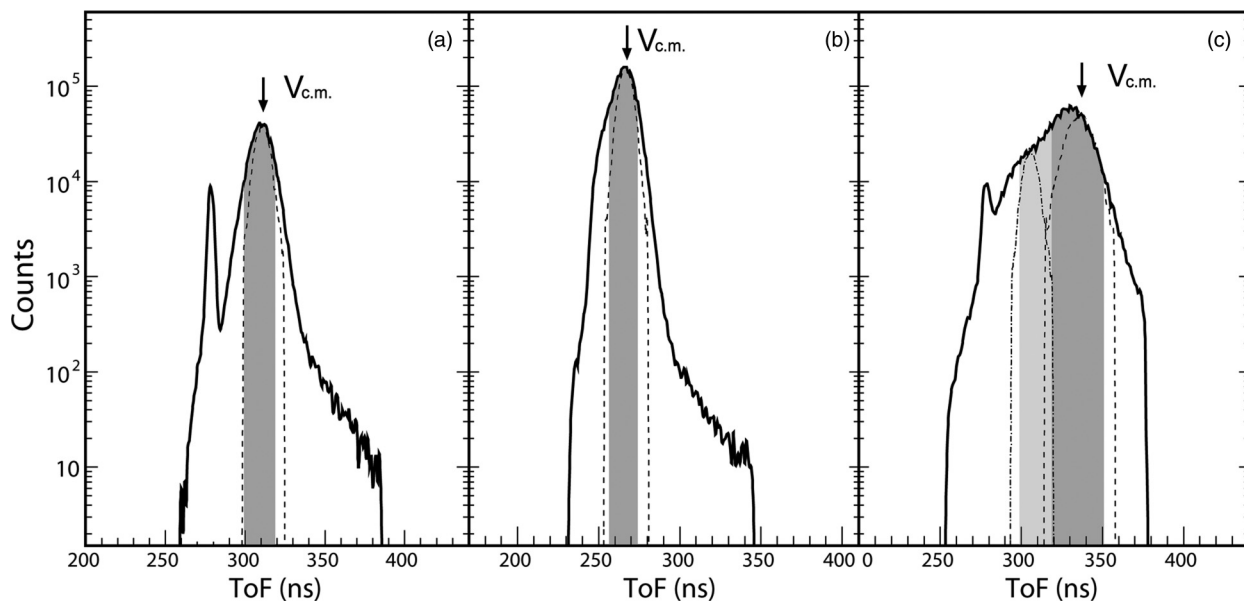
FIG. 3. Time-of-flight spectra of the evaporation residues measured in the reactions (a) ^{116}Sn + ^{12}C at $17A$ MeV, (b) ^{116}Sn + ^{12}C at $23A$ MeV, (c) ^{116}Sn + ^{24}Mg at $17A$ MeV. The shaded area represents the regions of events retained in the data analysis. A second region, indicated in light gray and corresponding to the one on the ^{12}C reaction at $17A$ MeV was selected in the study of the reaction ^{116}Sn + ^{24}Mg at $17A$ MeV to investigate the possible occurrence of dynamical effects. Dashed lines represent the results of GEMINI calculations performed as described in the text. The time-of-flight spectrum on ^{24}Mg is reproduced by the sum of two components associated with two different excitation energies.

ToF distribution compared to the ^{12}C one. Two components seem to be present in this case, a first component, in the region 320 to 350 ns, associated with flight times close to that corresponding to the center of mass (c.m.) [shown in dark gray in Fig. 3(c)] where the main peak of the distribution is observed and a second component [shown in light gray in Fig. 3(c)] associated with flight times similar to the one observed on the ^{12}C target at the same beam energy. The spectral shape can be accounted for by assuming, for ToF events close to the c.m., a fusion with the whole target followed by pre-equilibrium light-particle emission while shorter ToF can be associated with an incomplete fusion of about half of the target with the projectile, followed by pre-equilibrium emission and eventually evaporation.

In order to select a well-defined excitation energy, only events lying in a region of ±3% of the ToF peak, depicted by the gray shading in Fig. 3, were retained in the analysis and the study of light-charged-particle and γ-ray spectra was undertaken accordingly. A second region of ToF, similar to the one chosen in the study of the reactions ^{116}Sn + ^{12}C at $17A$ MeV was selected in the reaction on the ^{24}Mg target. If ToF information allows one to select events with different average momentum transfer, this shall be confirmed by the analysis of incomplete fusion events belonging to this second region which is expected to lead to a system similar to the one on the ^{12}C target at the same energy per nucleon. Furthermore, if dynamical effects are small, the study of the γ spectrum should exhibit characteristics similar to the one measured in complete fusion events from the ^{12}C target. This will be examined later in the paper.

In order to estimate the contribution of particle evaporation to the measured width of the ToF distribution, calculations

were performed with the code GEMINI++ [29] using as input to the code the excitation energies and masses of the hot system populated in the reactions as determined in Sec. III C. Results were then transformed in the laboratory reference frame and filtered including SOLE acceptance and magnetic-field transport effects down to the focal plane. The resulting distributions are displayed by dashed lines in Fig. 3. In the reactions with the ^{12}C target, particle evaporation is seen to account for the bulk of the width, confirming that the spread in excitation energy is very small. On the ^{24}Mg target instead, a larger difference is observed, with a tail on the shorter ToF side, suggesting the presence of different momentum transfers leading to a broader range of excitation energies. Including a second velocity distribution associated with the excitation of a lighter compound system similar to the one populated in the reaction on ^{12}C at $17A$ MeV leads to a better description of the overall ToF distribution supporting the idea of an incomplete fusion reaction with about half of the target nucleons.

B. Light-charged-particle analysis

In heavy-ion collisions at intermediate energies, light charged particles are emitted throughout the whole nucleus-nucleus collision, from the first nonequilibrated phase of the reaction where the more energetic particles are emitted to the later stages where statistical decay takes place. Their measurement can provide a better understanding of the reaction dynamics once the contributions from the different sources can be separated. Light-charged-particle spectra were measured in MEDEA in coincidence with evaporation residues for all reactions. In the data sorting, only fusion-like events belonging to the selected velocity windows were retained

and light-charged-particle kinetic-energy spectra were built accordingly.

In order to disentangle the contributions of the different emitting sources, the light-charged-particle energy spectra were reproduced through a fitting procedure assuming the isotropic emission from two moving sources. Only in the case of alpha particles, the spectra of the reactions ^{116}Sn + ^{12}C at $17A$ and $23A$ MeV were reproduced using the emission from a single source. The energy distribution of the emitted particles was parametrized, in the source rest frame, assuming a surface-type Maxwellian distribution given by

$$\frac{d^2M}{d\Omega dE} = \frac{M}{4\pi T^2}(E - E_c)\exp[-(E - E_c)/T], \quad (1)$$

where M is the multiplicity, T is the source temperature, and E_c is the Coulomb barrier. In order to fit the particle spectra the Maxwellian distribution is then transformed in the laboratory reference using the relation

$$\left[\frac{d^2M}{d\Omega dE}\right]_{\text{lab}} = \left(\frac{E_{\text{lab}}}{E'}\right)^{1/2}\left[\frac{d^2M}{d\Omega dE}\right]_{E=E'}, \quad (2)$$

where the particle energy E' in the source reference frame is given by

$$E' = E_{\text{lab}} + E_s - 2(E_{\text{lab}}E_s)^{1/2}\cos\theta_s, \quad (3)$$

where E_s indicates the energy of a particle moving with the source velocity. A χ^2 minimization procedure was adopted to extract, from the simultaneous fit of the spectra measured at different polar angles in MEDEA, the free parameters describing the main features of the emitting sources; namely, multiplicities, temperatures, and velocities, while the values of the Coulomb barriers were fixed to 1.0 and 3.0 MeV for the intermediate and compound nucleus source respectively in the case of protons and to 1.0 MeV in the case of alpha particles. However, the fit sensitivity to small variations of the Coulomb barrier values for both sources is rather small.

Proton spectra were extracted using all the rings of MEDEA in the region $42.4° < \theta_{\text{lab}} < 170°$. Only in the case of ^{116}Sn + ^{12}C reaction at $17A$ MeV proton spectra were build in the angular region $42.4° < \theta_{\text{lab}} < 119.5°$. They were simultaneously reproduced by a moving-source fit by assuming that particles are emitted from two sources, an intermediate-velocity source and a fast source. The existence of a third emitting source, associated in this case with the emission from a target-like fragment and frequently introduced in the fitting procedure to better reproduce the light-charged-particle spectra is not observed in this set of data. This can be understood considering that the ToF of the residues indicates the presence of almost complete fusion events or, in the case of incomplete fusion events on the ^{24}Mg target, that the target remnant is very small and weakly excited. Measured proton spectra and the associated fit, shown as a solid line, are displayed in Fig. 4. Good data reproduction has been obtained at all angles and for all the reactions investigated. The values of the parameters extracted from the fitting procedure are listed in Table I for both sources. The so-called intermediate source is characterized by a velocity v_{int} close to the half-beam velocity for all three reactions investigated. Such a value corresponds to the nucleon-nucleon center-of-mass velocity and is in good agreement with the systematics for reactions at intermediate energies [30]. The observed temperatures (or inverse slope) range from 7 MeV in ^{116}Sn reactions at $17A$ MeV to 8.2 MeV observed in ^{116}Sn + ^{12}C at $23A$ MeV. Such large values do not represent real temperatures but can be explained in terms of a random composition of the beam velocity with Fermi momenta of the nucleons of the colliding partners [31]. Deviation from this picture, observed especially at low beam energies, have been interpreted as a Pauli-blocking effect [31]. Proton multiplicities are observed to increase with beam energy and with the size of the participant region which in the case of the ^{24}Mg target is about a factor two larger than for the ^{12}C target. Further evidence of the dependence on
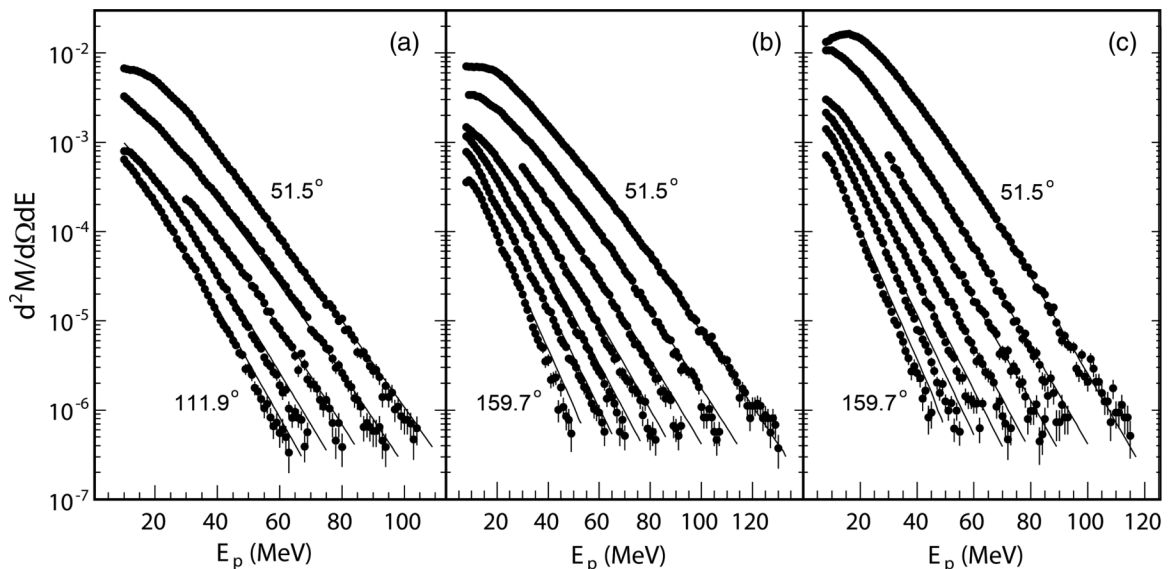
FIG. 4. Proton spectra detected with MEDEA in coincidence with evaporation residues in the reactions (a) ^{116}Sn + ^{12}C at $17A$ MeV, (b)^{116}Sn + ^{12}C at $23A$ MeV, and (c) ^{116}Sn + ^{24}Mg at $17A$ MeV. The solid lines are the result of the moving-source fit described in the text.

TABLE I. Values of multiplicity, temperature and velocity for intermediate and compound source as extracted from the fit of proton and α spectra detected in coincidence with evaporation residues for the three reactions.

	Reaction	Intermediate source			Compound source		
		M_{int}	T_{int} (MeV)	v_{int}/c	M_c	T_c (MeV)	v_c/c
proton	^{12}C - 17A MeV	0.4 ± 0.04	7.0 ± 0.2	0.10 ± 0.01	0.6 ± 0.06	3.7 ± 0.4	0.17 ± 0.02
proton	^{12}C - 23A MeV	0.7 ± 0.06	8.2 ± 0.2	0.11 ± 0.01	0.7 ± 0.06	4.1 ± 0.5	0.20 ± 0.03
proton	^{24}Mg - 17A MeV	0.8 ± 0.06	7.0 ± 0.2	0.10 ± 0.01	1.7 ± 0.10	5.0 ± 0.5	0.16 ± 0.02
proton	^{24}Mg - 17A MeV - 2nd bin	0.5 ± 0.05	6.4 ± 0.2	0.10 ± 0.01	0.8 ± 0.10	3.7 ± 0.5	0.17 ± 0.02
α	^{12}C - 17A MeV	0.5 ± 0.06	8.0 ± 0.2	0.10 ± 0.01			
α	^{12}C - 23A MeV	0.6 ± 0.06	9.0 ± 0.3	0.12 ± 0.01			
α	^{24}Mg - 17A MeV	1.1 ± 0.10	7.8 ± 0.3	0.10 ± 0.01	1.8 ± 0.20	5.0 ± 0.5	0.16 ± 0.03
α	^{24}Mg - 17A MeV - 2nd bin	0.9 ± 0.10	7.1 ± 0.3	0.10 ± 0.01			

the size of the participant region comes from the analysis of the proton spectra measured in coincidence with the window corresponding to lower momentum transfer. A multiplicity value similar to the one extracted from ^{12}C reaction at the same beam energy was extracted in agreement with a scenario in which the emitted protons mainly come from the first chance nucleon-nucleon collisions [15,30,32]. The main features of the source lead to an interpretation in which, in a multiple-source picture, the intermediate source represents a way to mimic the pre-equilibrium emission.

The fast source is instead characterized by a velocity slightly higher than the center-of-mass velocity for all three reactions. Fit values are in good agreement with the residue velocity measured using MACISTE ToF. Proton temperature varies from 3.7 MeV in the ^{116}Sn + ^{12}C reaction at 17A MeV to 5 MeV in the ^{116}Sn + ^{24}Mg reaction at 17A MeV while multiplicity increases accordingly from 0.6 to 1.7 (see Table I) clearly indicating this source as the compound nucleus source. The relative contribution of the two sources for a forward (51.5°) and a backward (97.1°) angle are presented for all the reactions in Fig. 5. Due to the inverse kinematics adopted, the contribution from the intermediate velocity source, shown as a dashed line, is the dominant one at all angles while the compound nucleus source, shown as a dotted line, gives a sizable contribution to the spectra only in the most forward angles becoming negligible already beyond 75°.

A similar fitting procedure was adopted to reproduce α-particle energy spectra. However, in the case of α particles, the spectra of the reactions ^{116}Sn + ^{12}C at 17A and 23A MeV were reproduced by using the emission from a single source, namely, the intermediate one while the introduction of a second source was needed to properly fit only the α spectra of the reaction on ^{24}Mg target. This is due to the fact that, in the reactions on ^{12}C target, the compound nucleus emission is strongly forward focused, outside the MEDEA detection acceptance. The reaction on the ^{24}Mg target instead has a slower compound system velocity and the emission, while being still forward focused, shows a measurable contribution already at polar angles $\theta = 51.5°$. α-particle spectra extracted in the angular region $42.4° < \theta_{lab} < 119.5°$ and their relative fit for all three reactions are displayed in Fig. 6. Data are well reproduced at all angles and for all the reactions investigated. The main features of the source used to reproduce the spectra

resemble those observed in the analysis of proton energy spectra. The velocity v_{int} shows values close to half-beam velocity for all three reactions, similar to those extracted in the proton fits. Temperatures are slightly higher than those extracted in the proton fit but display a similar trend, as observed in previous studies [15,25], increasing from about 8 MeV for reactions at 17A MeV to 9 MeV for the reaction at 23A MeV. Multiplicity values increase from 0.5 in the ^{116}Sn + ^{12}C reaction at 17A MeV to 1.1 in the ^{116}Sn + ^{24}Mg reaction at 17A MeV, as shown in Table I. Fit parameters of the fast source, introduced to properly fit data on the Mg target are in agreement with the main-source features extracted from proton spectra, confirming the existence of a contribution due to the emission from a hot compound system which is clearly evident only in the most forward ring of the setup (see Table I).

In order to perform a proper evaluation of pre-equilibrium emission which affects the excitation-energy determination, deuteron and triton contributions also have to be evaluated. The time resolution of 1.5 ns did not allow for a clean separation of deuterons and tritons and therefore only the sum energy spectra of the two species could be extracted. A fit of the sum energy spectra has been performed introducing two sources for deuterons (an intermediate and a compound one) and a single source for tritons. Source velocities have been fixed to the values extracted from the proton and α-particle spectra analysis. This approximate procedure has been adopted with the aim of estimating the deuteron and triton multiplicities and temperatures of the intermediate source to be used to evaluate the excitation energy and the mass of the hot recoiling nucleus formed in incomplete fusion events prior the evaporation stage. The results of the fit indicate that the multiplicity of deuterons emitted from the intermediate source ranges from 0.2 in the case of ^{116}Sn + ^{12}C at 17A MeV to 0.40 in the case of the ^{116}Sn + ^{24}Mg reaction. Similarly, the multiplicity of tritons emitted from the intermediate source ranges from 0.10 to 0.20. Possible errors in the relative yield of deuterons and tritons lead to a negligible difference in the excitation-energy determination due to the low multiplicity values measured. Temperature values of the intermediate source for deuterons are 7.7 MeV for 17A MeV reactions and 8.7 MeV in the case of 23A MeV reaction. In the fitting procedure, due to the low triton yield, the same temperature was assumed for deuterons and tritons.
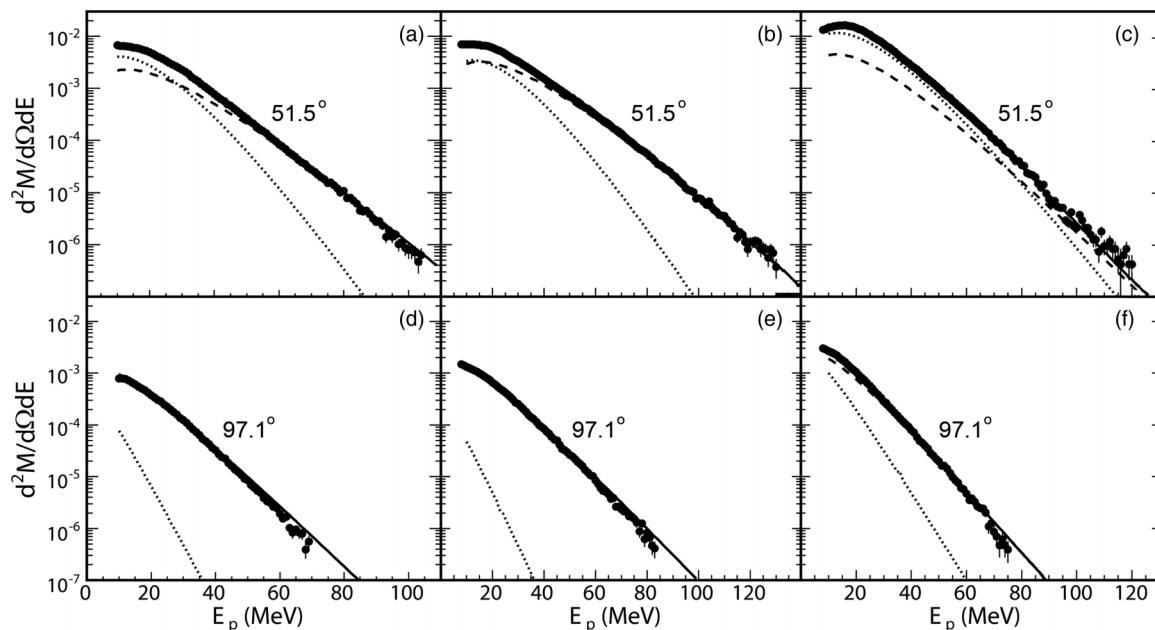
FIG. 5. Evolution of the contributions of the two Maxwellian sources adopted in the fit to the proton spectra detected in coincidence with evaporation residues at 51.5° and 97.1° in the reactions (a) ^{116}Sn + ^{12}C at 17A MeV, (b)^{116}Sn + ^{12}C at 23A MeV, (c) ^{116}Sn + ^{24}Mg at 17A MeV. Dashed and dotted lines represent respectively the contribution from the intermediate-velocity source and from the compound source. Solid line is the result of their sum.

While such a phenomenological approach allows us to reproduce the deuteron, triton, and α-particle spectra measured in heavy-ion collisions at intermediate energies and is a way to mimic the emission of particles originating at different timescales, the mechanism of particle production from the so-called intermediate source remains hidden in the large number of fit parameters. The intermediate source accounts, in fact, for dynamical emission described by early nucleon-nucleon collisions and by other pre-equilibrium process and it has been explained in the framework of a coalescence model where the

emission of light clusters is related to the momentum-space densities of the nucleons in the collision [30,33,34].

C. Excitation-energy determination

The study of light-charged-particle spectra together with the residue selection in ToF allows one to estimate the excitation energy of the hot system populated in the reaction after the pre-equilibrium stage. In order to infer this excitation energy for all three reactions we adopted a procedure similar to
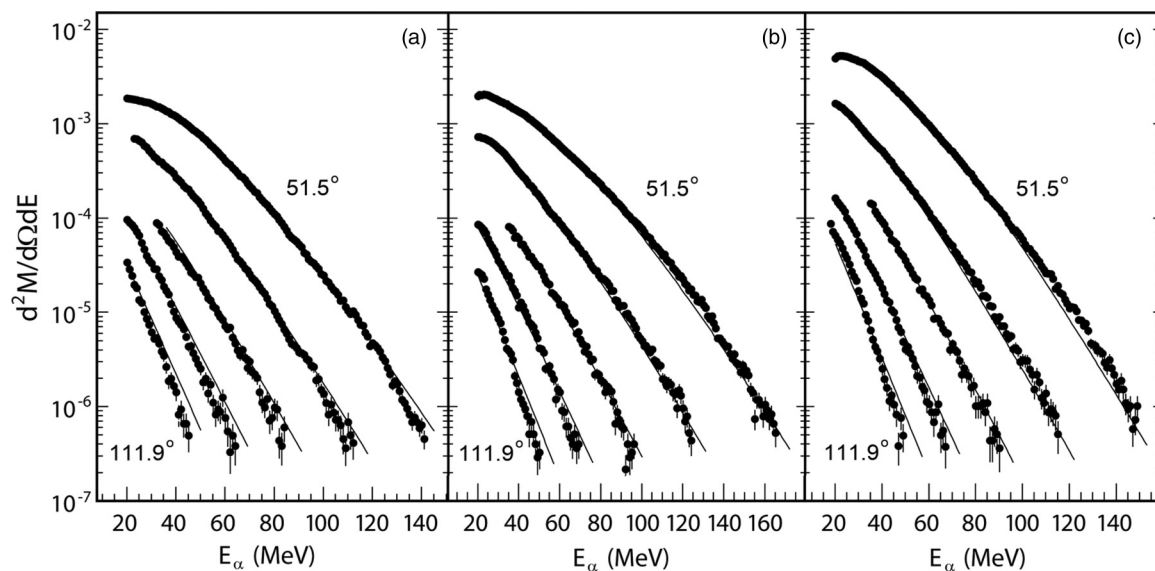
FIG. 6. Alpha-particle energy spectra detected in coincidence with evaporation residues in the reactions (a) ^{116}Sn + ^{12}C at 17A MeV, (b)^{116}Sn + ^{12}C at 23A MeV, and (c) ^{116}Sn + ^{24}Mg at 17A MeV. The solid lines are the result of the moving-source fit described in the text.

TABLE II. Values of average excitation energy, A, Z, and excitation energy per nucleon of the hot nuclei populated in the three reactions. Values were estimated taking into account the corrections for reaction Q values and pre-equilibrium emission.

Reactions	E_{beam}	E^* (MeV)	A	Z	E^*/A (MeV)
^{116}Sn + ^{12}C	$17A$ MeV	150 ± 10	124	54	1.21
^{116}Sn + ^{12}C	$23A$ MeV	190 ± 10	123	54	1.54
^{116}Sn + ^{24}Mg	$17A$ MeV	270 ± 20	132	58	2.04
^{116}Sn + ^{24}Mg - 2nd bin	$17A$ MeV	145 ± 10	123	53	1.18

the one described in Ref. [26]. Following this approach, the initial momentum transfer from projectile to the target was calculated by assuming a complete fusion reaction and then the measured amount of pre-equilibrium emission was removed. The amount of momentum removed by the different nuclear species was estimated from the multiplicities and velocities of the intermediate source extracted from the fit of light-charged-particle energy spectra. Since neutrons are not detected in the experiment, the pre-equilibrium neutron multiplicity was assumed equal to the proton one. This is a reasonable assumption if the pre-equilibrium proton emission is mainly accounted for in terms of first chance np collisions. [32,35]. By using momentum and energy conservation, the velocity, the mass, and the excitation energy of the compound system can be deduced. Corrections for energy losses in the target, and reaction Q values were also taken into account.

The velocities obtained from this procedure are slightly higher than the c.m. velocity and are in good agreement with the velocities extracted from the maxima of the ToF distributions measured. Excitation energies, excitation energies per nucleon, charges, and masses of the hot nuclei formed as deduced from the calculation are listed in Table II. The energy removed by the pre-equilibrium emission evaluated through the previously described procedure ranges from about 35 MeV for reaction on ^{12}C at $17A$ MeV to about 70 MeV for the reaction on ^{24}Mg at $17A$ MeV. Average mass loss ranges from four nucleons for the reaction on ^{12}C at $17A$ MeV to eight for the reaction on ^{24}Mg at $17A$ MeV. The amounts of energy and mass removed in the pre-equilibrium phase are much smaller than those estimated from the simple parametrization for pre-equilibrium emission, such as the one suggested in Ref. [36], showing the importance of experimentally determining the amount of pre-equilibrium emission for each reaction.

The overall procedure depicts a scenario where hot systems of similar masses were populated through incomplete fusion reactions in an excitation-energy range between 150 and 270 MeV, a region where the GDR quenching is expected to set in.

IV. γ-RAY SPECTRA

Gamma-ray spectra were measured in coincidence with fusion events for all the reactions. They display similar features: at low energies an exponentially decreasing component associated with the statistical emission from the compound nucleus at the end of the decay chain, a pronounced bump around 14 MeV corresponding to the decay of the GDR excited in

nuclei of mass $A \approx 130$ and, above ~ 35 MeV, an exponentially decreasing component due to the bremsstrahlung radiation arising mainly from first chance np collisions in the first, nonequilibrated, stages of the reaction.

Figure 7 shows the γ spectra measured in coincidence with fusion events for the three systems investigated. The spectra are built by summing the contribution of detectors in the two rings centered at $83°$ and $97°$ where the doppler shift is negligible. They represent the differential γ multiplicity normalized over 4π per fusion event. For each reaction the number of fusion events was obtained from a normalization run where inclusive data for residues were collected triggering only with MACISTE focal plane detector.

A. High-energy component

In order to study the GDR properties, the bremsstrahlung contribution has to be evaluated and subtracted from the spectra. The np bremsstrahlung contribution was evaluated by fitting the high-energy part of the γ spectra ($E_\gamma > 35$ MeV) by an exponential function having slope and intensity as free parameters. The results of the fitting procedure are shown in Fig. 7(a) as solid lines. Due to the large statistics collected an accurate determination of the slopes was possible. The values of the slope extracted from the fits are equal to 7.9 ± 0.3 MeV on ^{12}C and 8.3 ± 0.3 MeV on the ^{24}Mg target for $17A$ MeV reactions while a higher value of 9.5 ± 0.3 MeV was found on the ^{12}C target for the reaction at $23A$ MeV (see Table III). This beam-energy dependence of the slope parameter exhibits agreement with the systematics for nucleon-nucleon bremsstrahlung which shows a dispersion of the data around the average trend of E_0 given by the relation $E_0 = 0.68 E_{cc}^{0.83}$ where $E_{cc} = E_{\text{beam}} - V_c/A_p$ is the reduced bombarding energy, V_c is the Coulomb barrier, and A_p is the projectile mass [37,38].

The high-energy γ-ray yield was extracted by integrating the spectra for energies above 35 MeV (see Table III). The difference in the yield between the reactions at $17A$ MeV reflects the size of the participant zone and can be understood in the framework of a simple geometrical model. In fact, in the first nucleon-nucleon collision hypothesis, the high-energy γ multiplicity is given by the simple relation $M_\gamma = N_{np}(b)P_\gamma$ where $N_{np}(b)$ represents the number of np collisions in the overlap region which is impact-parameter dependent and can be calculated in the framework of geometrical model while P_γ is the probability to produce a bremsstrahlung photon [39]. Due to the choice of the integration window it corresponds to the probability to produce a γ ray with energy higher than or equal to 35 MeV. Complete or close to complete fusion events like the ones selected in this experiment can be mainly associated with central collisions and, due to the strong mass asymmetry between projectile and target, a full overlap between colliding nuclei can be assumed to estimate the size of the participant zone. Within this assumption the observed difference in high-energy γ multiplicity can be fully explained as due to the higher average number of np collisions in the participant zone for ^{24}Mg target compared to ^{12}C. In fact, $P_{\gamma>35\text{MeV}}$ values extracted for both reactions are similar, being 2.2×10^{-6} for ^{12}C and
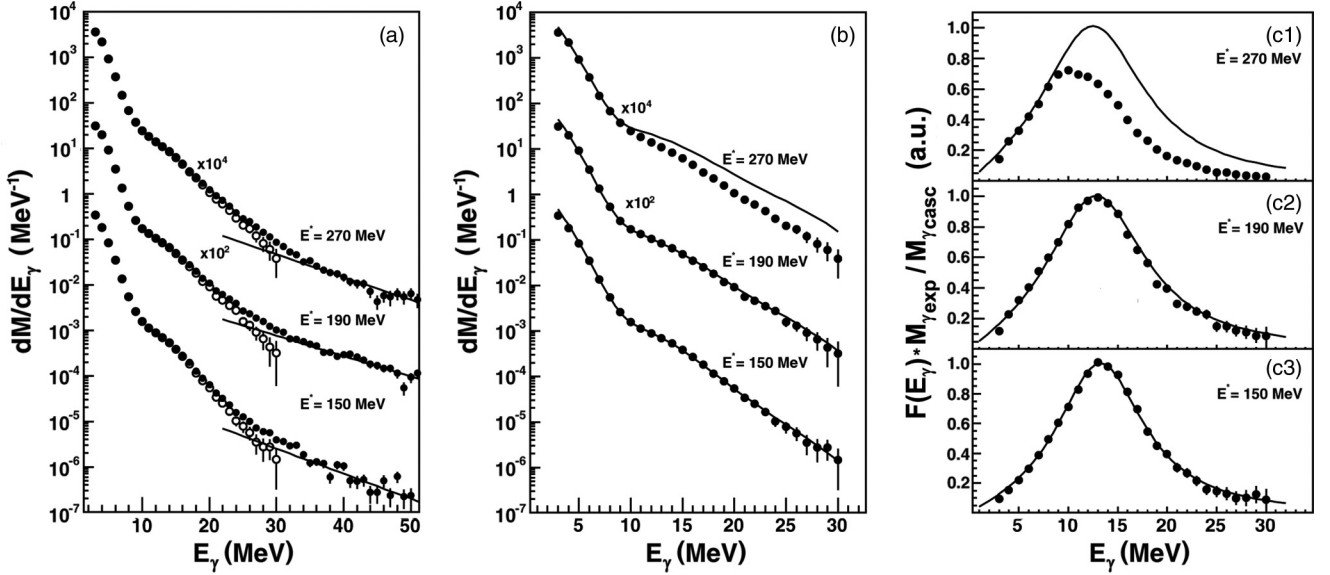
FIG. 7. (a) Solid symbols represent the γ spectra measured around $90°$ for the three reactions investigated and correspond to excitation energies of $E^* = 150$, 190, and 270 MeV. They represent the differential γ multiplicity normalized over 4π per fusion event. Solid lines represent the fit of the bremsstrahlung component for $E_\gamma \geqslant 35$ MeV. Open symbols represent the γ spectra after subtraction of bremsstrahlung contribution. (b) Comparison of the γ spectra after bremsstrahlung subtraction with statistical model calculations shown as full lines. (c) Linearized spectra (see text) compared with Lorentzian function used, in statistical model calculations, to describe GDR decay (solid line).

2.0×10^{-6} for the ^{24}Mg target. A $P_{\gamma>35\text{MeV}} = 7.8 \times 10^{-6}$ was instead extracted from the analysis of the reaction on ^{12}C at $23A$ MeV. All values are in agreement with the systematics of $P_{\gamma>30\text{MeV}}$ variation as a function of E_0 once the proper scaling factor to correct for the different energy threshold is applied [38].

The exponential function is then extrapolated down to low energies and subtracted from each spectrum in order to obtain the statistical γ component displayed in Fig. 7(a) as open symbols. The error bars include the statistical error and the errors on the subtraction of the bremsstrahlung component due to uncertainties on the slope and normalization.

B. Statistical model calculations

Gamma rays from GDR decay can be emitted at all steps during the deexcitation process, which involves nuclei at different mass and excitation energy due to particle evaporation. Moreover, the various reactions studied here as in previous investigations lead to initial hot nuclei with different masses and spins. Therefore an investigation of the evolution of the

TABLE III. Values of inverse slope (E_0) and multiplicity of γ rays (M_γ) as extracted from the fit of γ spectra above 35 MeV for all the reactions.

Reactions	E_{beam}	E_0	M_γ (10^{-5})
^{116}Sn + ^{12}C	$17A$ MeV	7.9 ± 0.3	1.2 ± 0.1
^{116}Sn + ^{12}C	$23A$ MeV	9.5 ± 0.3	4.2 ± 0.1
^{116}Sn + ^{24}Mg	$17A$ MeV	8.3 ± 0.3	2.1 ± 0.1
^{116}Sn + ^{24}Mg - 2nd bin	$17A$ MeV	8.0 ± 0.4	1.1 ± 0.2

GDR yields as a function of excitation energy must rely on a comparison with statistical calculations taking into account the whole decay sequence. Our benchmark here is the statistical decay code DCASCADE [40,41] which treats the statistical emission of γ rays, neutrons, protons, and α particles from an equilibrated compound nucleus with a given excitation-energy, mass, and spin range.

It was shown in Sec. III A that the width of the ToF bins for which the spectra were extracted can be mostly accounted for by the broadening due to particle evaporation. Therefore it is reasonable to assume a single value of excitation energy for each case. The initial excitation energies, nuclear charges, and masses used as input to DCASCADE are listed in Table II. Triangular spin distributions were used in the calculations with a maximum angular momentum leading to fusion J_{max}, calculated internally by the code, of $62\hbar$, $68\hbar$, and $70\hbar$ for the three reactions respectively and a diffuseness equal to $2\hbar$. Calculations were also performed using a single spin value rather than a distribution. In this case a spin value $J = 50\hbar$ was used in the calculation for all the reactions investigated. However, no significant differences were observed in the main GDR parameters using the two different approaches and therefore the conclusions are independent of the spin distribution used. A Lorentzian lineshape was assumed for the GDR and the strength was taken equal to 100% of the Thomas–Reiche–Kuhn (TRK) sum rule. It is worth noting that the DCASCADE program was slightly modified to calculate at each decay step the GDR strength which depends linearly on NZ/A. For the cases at E^* of 150 and 190 MeV, E_{GDR} and Γ_{GDR} were determined by a best fit to the data. E_{GDR} turns out to be 14.3 ± 0.3 MeV in both cases while Γ_{GDR} increases from 11.0 ± 0.8 MeV to 12.5 ± 1.0 MeV between 150 and 190 MeV excitation energy. These values are slightly

smaller than those obtained for similar cases in Ref. [5]. The errors on the GDR width and centroid were estimated using a χ^2 minimization procedure considering the spectrum energy region between 9 and 30 MeV. They include both a 10 MeV error on the excitation-energy determination and a $\Delta A = \pm 1$, $\Delta Z = \pm 1$ on the average mass and/or charge of the system. Error values represent fits displaying a χ^2 value a factor two larger than the one obtained in the best fit. Since, in the calculation, the bulk of the GDR γ rays are emitted during the first steps of the decay, the use of a width decreasing below $E^* = 120$ MeV, and following the experimental trend [42], does not significantly change the results.

An important input in the statistical model calculations is the level density parameter. Different measurements have shown a marked variation of the level density parameter as a function of the system temperature or excitation energy [25,43]. Due to the large values of excitation energy involved in this set of measurements, a proper reproduction of the γ spectrum calls for a use of a level density parameter dependent on the temperature during the decay process of the hot system. The parametrization suggested by Ormand *et al.* who propose a level density parameter varying from $a = A/8.5$ MeV^{-1} at $T = 0$ MeV to $a = A/12$ MeV^{-1} at $T = 5$ MeV [44] was adopted in the calculations. Shell effects are taken into account by using the Reisdorf formalism based on the Ignatyuk expression for the level density [41,45,46].

The results of the CASCADE calculations, folded with the response function of the BaF$_2$ detectors [47], are shown as full lines in Fig. 7(b) and compared to the experimental spectra after bremsstrahlung subtraction. Note that there is no arbitrary normalization involved in the comparison. At $E^* = 150$ and 190 MeV the agreement between calculation and data is remarkably good over more than five orders of magnitude in cross section and down to 3 MeV γ energy, showing that the inputs of DCASCADE are well under control and demonstrating once again that there is no γ-ray quenching up to 190 MeV excitation energy which corresponds, for the system investigated, to 1.5 MeV/A. In order to better judge the quality of the reproduction, the linearized spectra $(M_{\gamma-\text{expt}}/M_{\gamma\text{-CASCADE}})F(E_\gamma)$ are plotted in Fig. 7(c) and compared to $F(E_\gamma)$, where $F(E_\gamma)$ is the Lorentzian function used in DCASCADE arbitrarily normalized to one.

At the highest excitation energy of 270 MeV it is no longer possible to fit the centroid energy and the width of the GDR because no reasonable parameter set leads to a good reproduction of the data. Therefore we have performed the calculation with $E_{\text{GDR}} = 14$ MeV and $\Gamma_{\text{GDR}} = 13$ MeV. The centroid energy was chosen scaling according to $A^{-1/3}$ the best fit value of 14.3 MeV obtained above by the estimated mass of the excited system. The width was extrapolated from the values fit at lower excitation energy according to the trend measured in Ref. [5]. The calculation at 270 MeV overshoots the data in the GDR region, indicating the onset of the GDR quenching, while the low-energy region is still well reproduced up to 10 MeV γ energy. This is clearly confirmed by observation of the linearized spectrum. It has been checked that no reasonable variation of any of the input parameters can restore a good agreement between calculation and data. In fact, with increasing excitation energy the statistical model predicts

an increase of GDR yield due to the higher number of decay step for the GDR γ decay to compete with particle emission in the cascade process down to zero while in the experimental data a saturating trend of the γ multiplicity starts to appear. This demonstrates that onset of the GDR quenching takes place slightly above 200 MeV excitation energy in this mass region which should be a stringent constraint on any model of the GDR in nuclei at high temperatures.

The sensitivity of the results to the level density parameter adopted in the calculation has been investigated by comparing statistical model calculations for the different reactions performed varying only the level density parameter. Fixed level parameters $a = A/K$ as well as Lestone [48,49] and Ormand parametrizations of the level density as a function of excitation energy were used. Using a constant level density parameter slightly influences the spectral shape. Data at $E^* = 150$ MeV can be reproduced by using $a = A/10.8$ MeV^{-1} while $a = A/11.5$ MeV^{-1} gives a better description of the data at $E^* = 190$ MeV. In both calculations a width about 0.8 MeV larger than the one used to fit the data using Ormand parametrization is needed to reproduce the data. At $E^* = 270$ MeV all reasonable hypotheses for the level density lead to an overestimate of GDR yield and therefore the conclusions drawn above are not affected by a specific choice. On the other hand, the comparison between data and calculations at 150 and 190 MeV where no quenching is observed supports the choice of the Ormand level density prescription.

In the attempt to simulate the γ spectrum in a simple way we introduced in DCASCADE a sharp suppression of the γ emission above a given excitation energy, the so-called sharp cutoff. Different calculations were performed using the same values of strength, centroid, and width for the GDR emission used at $E^* = 270$ MeV. Data can be reasonably well reproduced by assuming a cutoff value of 230 MeV, as shown by the full line in Fig. 8 which corresponds to a limiting excitation energy per nucleon $E^*/A \sim 1.7$ MeV/A. A similar result was found in the analysis of the reaction ^{40}Ar + ^{92}Zr populating a hot system of mass $A = 126$ at $E^* = 280$ MeV [50,51]. While such an approach points to a sudden disappearance of the GDR above the cutoff value, the precise shape of the cutoff cannot be inferred because different types of smooth cutoff predicting a progressive disappearance of GDR as a function of excitation energy could also reproduce the data trend [9–13].

In order to investigate a possible entrance channel effect on the results, the γ-ray spectrum from the ^{116}Sn + ^{24}Mg reaction at $17A$ MeV was extracted in coincidence with a residue time-of-flight bin corresponding to fusion of half of the target, i.e., ^{12}C. In the absence of entrance channel effects, this spectrum, displayed as open circles in Fig. 9 after bremsstrahlung subtraction, should be identical to that from the ^{12}C-induced reaction at the same energy per nucleon shown again for comparison in the same figure as open circles. The statistical model calculation performed for the ^{12}C-target case, shown as a solid line, reproduces very well the spectrum from the ^{24}Mg target reaction in the GDR region, confirming our understanding of the incomplete fusion reaction and the determination of the excitation energy. A small excess of strength is however observed at lower γ-ray energies and its origin is not yet understood.
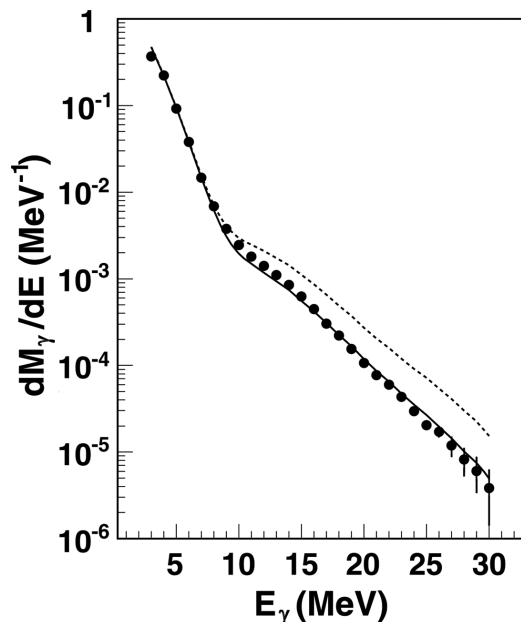
FIG. 8. Comparison of γ spectrum corresponding to $E^* = 270$ MeV excitation energy with statistical model calculations. Standard statistical model calculation is shown as dashed line while a calculation assuming a sharp cutoff of the γ-ray emission above $E^* = 230$ MeV is shown as a full line.

C. γ-ray spectra from ^{36}Ar + ^{98}Mo reaction at $37A$ MeV

In order to map the progressive evolution of the GDR features as a function of excitation energy it is interesting to extend the comparison to higher excitation energies. For this purpose, data obtained in the study of ^{36}Ar + ^{98}Mo reaction at $37A$ MeV performed at GANIL [18] were re-analyzed by using
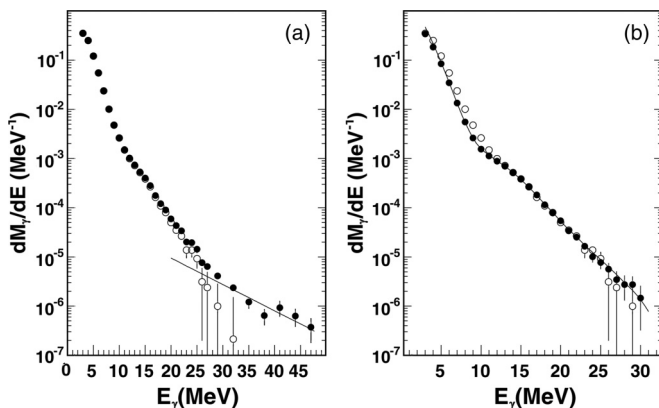
FIG. 9. (a) Solid symbols represent the γ spectra measured around $90°$ for the reaction ^{116}Sn + ^{24}Mg in coincidence with a residue time-of-flight bin corresponding to fusion of half of the target. Solid line represents the fit of the bremsstrahlung component for $E_\gamma \geqslant 35$ MeV. Open circles represent the γ spectra resulting from the subtraction of bremsstrahlung contribution. (b) Open circles represent the γ spectra after subtraction of bremsstrahlung contribution, shown in panel (a). For comparison, the γ spectrum of the reaction ^{116}Sn + ^{12}C is shown as full circles. The statistical model calculation is shown as full line.

the new version of the CASCADE code (DCASCADE), in order to depict a coherent scenario of the GDR evolution properties using the same code as a reference. In this experiment light charged particles and γ-rays were detected with MEDEA in coincidence with evaporation residues detected using two parallel plate avalanche counters (PPACs) covering polar angles from $6°$ to $22°$. Evaporation residues were identified by combining time-of-flight and energy-loss information. The ToF spectrum of evaporation residues shows a broad distribution which reflects the combined effects of different momentum transfers corresponding to different excitation energies and the broadening due to the evaporation stage.

Data were sorted in three bins in ToF and the excitation energies were estimated from the residue velocities through the massive transfer model [52] correcting for pre-equilibrium light-charged-particle emission as described in Ref. [15]. Average excitation energies of 300, 350, and 430 MeV were deduced for the hot systems populated in each bin, with masses of 105, 108, and 111, respectively [15]. γ-ray energy spectra were built by summing over all the detectors of the rings placed around $90°$ [18] and were compared with statistical model calculations performed using the DCASCADE code. The GDR decay was computed in the code by assuming that, for all excitation energies, $E_{GDR} = 15$ MeV, $\Gamma_{GDR} = 13$ MeV, and $S_{GDR} = 100\%$ EWSR for the energy, width, and strength of the GDR. A level density parameter dependent on the temperature of the system was adopted following the parametrization suggested by Ormand *et al.* [44], similarly to what previously done for data at lower excitation energies. The results of the calculations folded with detector response are shown in Fig. 10. Also, in this case no arbitrary normalization to the data was used. The calculations are slightly different from those presented in Ref. [18] for the same data set, the differences being ascribed to a re-analysis with an updated version of the CASCADE code in which the GDR strength was recalculated at each step of the decay chain [40,41]. The comparison shows that the calculations strongly overpredict the data in the GDR region at all excitation energies while the low-energy region is still reasonably well reproduced. The effect increases with the excitation energy of the system.

Following the approach previously used for the 270 MeV data, calculations with a sharp cutoff of the γ emission were performed to reproduce the spectra. GDR parameters were kept fixed to the values used in the standard statistical calculations. Gamma spectrum at $E^* = 350$ MeV can be reasonably well reproduced with a cutoff value of 230 MeV while a value of 220 MeV was instead used for the two other excitation energies, as shown in Fig. 10. This result, while being slightly lower than the value of 250 MeV extracted from the $27A$ MeV data [8], confirms the existence of a limiting excitation energy for the collective motion that, for nuclei of mass $A \sim 108$, corresponds to $E^*/A \sim 2.1$ MeV. The differences observed in the cutoff values extracted in different data sets could be ascribed to the different version of the code used to reproduce the γ spectra.

The existence of a limiting excitation energy for the collective motion can be qualitatively understood by assuming that, above a certain excitation energy, the equilibration time of the collective oscillation becomes longer than the particle
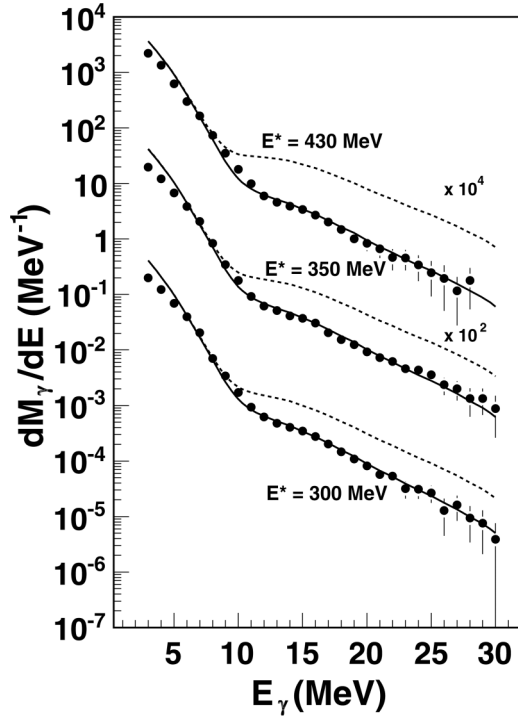
FIG. 10. Gamma spectra after bremsstrahlung subtraction for the three velocity bins corresponding to excitation energies of $E^* = 300$, 350, and 430 MeV and relative statistical model calculations shown as dashed lines. Full lines correspond instead to statistical model calculation assuming a sharp cutoff value of the γ emission equal to 220 MeV for $E^* = 300$ and 430 MeV and to 230 MeV for $E^* = 350$ MeV.

FIG. 11. (a) GDR γ-ray multiplicities integrated in the region 12–20 MeV as a function of excitation energy per nucleon for the different reactions investigated. Full symbols represent the GDR γ multiplicity measured in the $17A$ and $23A$ MeV reactions while open symbols represent instead the GDR γ multiplicity measured in the reaction ^{36}Ar + ^{98}Mo. Full lines indicate the multiplicities extracted from CASCADE calculations relative to each reaction obtained integrating the spectra in the energy region 12–20 MeV. (b) Ratio of the experimental GDR γ multiplicity to CASCADE multiplicity shown in panel (a) as a function of excitation energy per nucleon.

emission time leading to a progressive suppression of the GDR γ emission. A clear picture emerges from this data spanning a large excitation-energy range ($E^* = 150$ to 430 MeV). Full GDR strength is observed at low excitation energies while a deficit of the γ multiplicity with respect to predictions for 100% EWSR is observed to appear above $E^* = 200$ MeV and to increase regularly with increasing excitation energy.

V. GIANT-DIPOLE-RESONANCE YIELD EVOLUTION

In an attempt to quantify the observation of a progressive GDR quenching observed comparing data and statistical model calculations, the experimental spectra and CASCADE calculations were integrated between 12 and 20 MeV; the energy region where the GDR emission is concentrated. The extracted yields are shown in Fig. 11(a) as a function of excitation energy per nucleon. Data from the reactions at $17A$ and $23A$ MeV are shown as full symbols while data from $37A$ MeV reaction are shown as open symbols. For the three lowest excitation-energy points the integrated γ multiplicity is observed to increase from $(3.2 \pm 0.2) \times 10^{-3}$ to $(5.2 \pm 0.2) \times 10^{-3}$. The quoted errors include statistical errors, the estimated error on the bremsstrahlung subtraction, and a contribution related to uncertainties in the normalization. The comparison with the GDR yield extracted from CASCADE calculation connected by solid lines in Fig. 11(a) shows that the absolute values and

the trend are well reproduced with exception of the highest excitation-energy point which starts to fall below the CASCADE calculation. The yields extracted from the three velocity bins of $37A$ MeV data are lower than the values extracted at lower excitation energies, the values being $(2.6 \pm 0.2) \times 10^{-3}$, $(2.8 \pm 0.2) \times 10^{-3}$, and $(2.6 \pm 0.3) \times 10^{-3}$ for $E^*/A = 2.8$, 3.2, and 3.9 MeV, respectively [Fig. 11(a)]. The comparison with the respective CASCADE calculations connected by solid lines in Fig. 11(a) shows that the experimental data fall largely below the continuously increasing CASCADE values indicating the quenching of the GDR with increasing excitation energy per nucleon. The break observed between the two sets of data is due at least in part to the different nuclei populated in the two sets of reactions whose mass A and charge Z influence the value of the NZ/A factor in the formula of decay width for statistical $E1\gamma$ decay. In an attempt to remove this dependency and to make the comparison between data sets possible, the ratios between the experimental and calculated yields for each excitation energy per nucleon were calculated. Results are displayed in Fig. 11(b) as a function of excitation energy per nucleon for all the reactions investigated. A smooth decrease of this quantity is observed, starting above 1.5 MeV and continuing up to the highest energy measured indicating

a quenching of the GDR which seems to set in around 2 MeV excitation energy. It is important to note once again that the quantity displayed corresponds to an integration of the γ yield over the full decay chain starting at the E/A indicated, and should not be interpreted as a reduction factor of the yield at a given excitation energy.

VI. MASS DEPENDENCE OF LIMITING EXCITATION ENERGY FOR COLLECTIVE MOTION

Heavy-ion collisions provide a powerful tool to probe hot and dense phases of nuclear matter whose features are still under debate and investigation. In particular, in the last decade, the study of the nuclear caloric curve, i.e., the relation between the system temperature and its excitation energy, has yielded evidence of a trend that is reminiscent of liquid water heating to the boiling point, the plateau region being interpreted as a liquid-gas phase transition in nuclear matter [43,53]. Other possible signatures of a liquid-gas phase transition or critical behavior in nuclei were found by using different experimental probes and theoretical approaches [54–57]. It has been proposed that the presence of collective states can be a signature of the existence of a compound nucleus and that the disappearance of the collective motion at high excitation energies could therefore provide further evidence for a phase transition in nuclei [58,59]. From this point of view, probing the limits for the collective behavior in nuclei represents a further way to get information on the liquid-gas phase transition and to extract complementary information to the caloric curve studies.

Data on the nuclear caloric curve, collected over a wide range of nuclei, show that the temperature at which the plateau region sets in decreases as a function of the nuclear mass [43]. This affects the excitation-energy value of the transition point from a Fermi-gas-like behavior to a plateau region which decreases with increasing mass from about 8 MeV for nuclei with mass $A = 30$ to 60 to about 3 MeV for nuclei of mass $A = 180$ to 240, as shown in Fig. 12 [43]. A similar trend can be observed studying the limiting excitation energy for the collective motion as a function of the nuclear mass even if data were extracted up to now only in two different mass regions, $A = 60$ to 70 and $A = 105$ to 135,
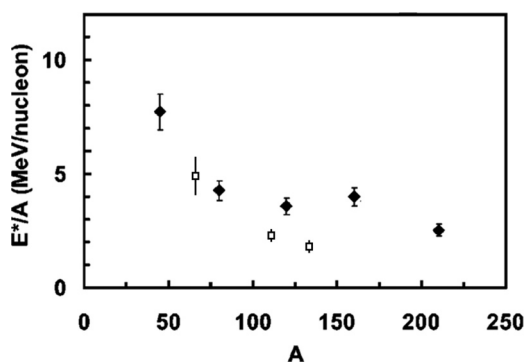
FIG. 12. Excitation energy per nucleon at which the limiting temperature is reached as a function of the system mass [43]. Open symbols show the limiting excitation energies per nucleon for the collective motion extracted in different mass regions.

the region investigated in the present paper. Measured values, plotted as open symbols in Fig. 12, vary significantly with mass, being $E^*/A \simeq 5$ MeV in the mass region $A = 60$ to 70 [60,61], about 2.1 MeV in the mass region $A = 105$ to 111 and about 1.7 MeV for nuclei with mass $A \simeq 132$. It is interesting to observe that the limiting excitation energies for the collective motion extracted from GDR studies are close to the energies where the plateau of the caloric curve, built in the similar mass region, sets in. This intriguing feature suggests the possible occurrence of a transition from order to chaos in nuclei for excitation energies close to the values where signals of a liquid-gas phase transition were claimed to be present. However, one should also point out that the observed trend could be interpreted in a different way. The GDR quenching appears, in fact, in both mass regions at about the same excitation energy, namely $E^* = 220$ to 250 MeV, which could also be the driving parameter governing the quenching. In such a case the measured values could be simply related to the competition between the different timescales which come into play, population and decay of the collective motion on one side and thermalization and decay of the hot system on the other without any particular link with a phase transition.

VII. CONCLUSIONS

The evolution of the GDR properties in hot nuclei of mass $A \sim 130$ was investigated through the study of three different reactions at $17A$ and $23A$ MeV. Hot nuclei were populated in an excitation-energy range between 150 and 270 MeV through complete and incomplete fusion reactions. Events were selected by applying a cut in recoil velocity for each reaction investigated and data analysis was performed accordingly. Excitation energies and masses of the compound systems were determined by combining ToF information together with the analysis of the light-charged-particle energy spectra to evaluate the amount of pre-equilibrium emission. The analysis of the γ spectra shows the presence of a bump centered at 14 MeV associated with the GDR decay. Evolution of the GDR features was extracted through a comparison with statistical model calculations performed with an updated version of the CASCADE code. We found that a very good reproduction of the experimental data is obtained up to $E^* = 190$ MeV while evidence of a quenching of the GDR γ yield appears in the data at $E^* = 270$ MeV. Such an effect becomes progressively more important when the comparison is extended to $37A$ MeV data, indicating the existence of a limiting excitation energy for the collective motion of about $E^*/A = 2.1$ MeV for nuclei of mass $A = 105$ to 111 and of about 1.7 MeV for nuclei of mass $A \sim 132$. Evidence of a limiting excitation for the collective motion was also extracted in nuclei of mass $A = 60$ to 70 but the value of about $E^*/A \simeq 5$ MeV differs significantly from those measured for nuclei in the mass region $A = 105$ to 135, suggesting the existence a mass dependence of the limiting excitation energy per nucleon for the collective motion. Interesting similarities in trend and absolute values can be found when comparing the limiting excitation energy for the collective motion with the energy at which the plateau of the caloric curve sets in,

indicating the onset of a liquid-gas phase transition. This feature suggests a possible link between GDR disappearance and the liquid-gas phase transition which deserves further investigation from both theoretical and experimental points of view. In particular, extending the systematics of the GDR to hot nuclei with $A = 160$ to 180 could provide further information on the possible link between GDR disappearance

and liquid-gas phase transition and therefore shed additional light on the mechanism responsible for the GDR quenching.

[1] D. Santonocito and Y. Blumenfeld, Eur. Phys. J. A **30**, 183 (2006).

[2] P. F. Bortignon, A. Bracco, and R. Broglia, *Giant Resonances: Nuclear Structure at Finite Temperature* (Harwood Academic Publishers, Amsterdam, 1998).

[3] M. N. Harakeh and A. van der Woode, *Giant Resonances: Fundamental High-Frequency Modes of Nuclear Excitations* (Oxford Science Publications, New York, 2001).

[4] E. Ramakrishnan, T. Baumann, A. Azhari, R. A. Kryger, R. Pfaff, M. Thoennessen, S. Yokoyama, J. R. Beene, M. L. Halbert, P. E. Mueller, D. W. Stracener, R. L. Varner, R. J. Charity, J. F. Dempsey, D. G. Sarantites, and L. G. Sobotka, Phys. Rev. Lett. **76**, 2025 (1996).

[5] O. Wieland *et al.*, Phys. Rev. Lett. **97**, 012501 (2006).

[6] J. J. Gaardhøje, A. M. Bruce, J. D. Garrett, B. Herskind, D. Barnéoud, M. Maurel, H. Nifenecker, J. A. Pinston, P. Perrin, C. Ristori, F. Schussler, A. Bracco, and M. Pignanelli, Phys. Rev. Lett. **59**, 1409 (1987).

[7] K. Yoshida, J. Kasagi, H. Hama, M. Sakurai, M. Kodama, K. Furutaka, K. Ieki, W. Galster, T. Kubo, and M. Ishihara, Phys. Lett. B **245**, 7 (1990).

[8] J. H. Le Faou *et al.*, Phys. Rev. Lett. **72**, 3321 (1994).

[9] P. F. Bortignon, A. Bracco, D. Brink, and R. A. Broglia, Phys. Rev. Lett. **67**, 3360 (1991).

[10] P. Chomaz, Nucl. Phys. A **569**, 203c (1994).

[11] P. Chomaz, Phys. Lett. B **347**, 1 (1995).

[12] A. Smerzi, A. Bonasera, and M. Di Toro, Phys. Rev. C **44**, 1713 (1991).

[13] K. A. Snover, Nucl. Phys. A **687**, 337c (2001).

[14] E. Migneco, C. Agodi, R. Alba, G. Bellia, R. Coniglione, A. Del Zoppo, P. Finocchiaro, C. Maiolino, P. Piattelli, G. Raia, and P. Sapienza, Nucl. Instrum. Methods Phys. Res., Sect. A **314**, 31 (1992).

[15] D. Santonocito *et al.*, Phys. Rev. C **66**, 044619 (2002).

[16] A. Del Zoppo, C. Agodi, R. Alba, G. Bellia, R. Coniglione, P. Finocchiaro, C. Maiolino, E. Migneco, A. Peghaire, P. Piattelli, and P. Sapienza, Nucl. Instrum. Methods Phys. Res., Sect. A **327**, 363 (1993).

[17] T. Suomijärvi *et al.*, Phys. Rev. C **53**, 2258 (1996).

[18] D. Santonocito, Y. Blumenfeld, C. Agodi, R. Alba, G. Bellia, R. Coniglione, F. Delaunay, A. Del Zoppo, P. Finocchiaro, N. Frascaria, F. Hongmei, V. Lima, C. Maiolino, E. Migneco, P. Piattelli, P. Sapienza, and J. A. Scarpaci, Nucl. Phys. A **788**, 215c (2007).

[19] G. Bellia, P. Finocchiaro, K. Loukachine, C. Agodi, R. Alba, L. Calabretta, R. Coniglione, A. Del Zoppo, C. Maiolino, E. Migneco, P. Piattelli, G. Raciti, D. Rifuggiato, D. Santonocito, and P. Sapienza, IEEE Trans. Nucl. Sci. **43**, 1737 (1996).

[20] U. Mosel, in *Treatise on Heavy-Ion Science—Fusion and Quasi-Fusion Phenomena*, edited by D. Allan Bromley (Plenum Press, New York, 1984), Vol. 2, p. 3.

[21] S. Chakrabarty, B. S. Tomar, A. Goswami, G. K. Gubbi, S. B. Manohar, Anil Sharma, B. Bindukumar, and S. Mukherjee, Nucl. Phys. A **678**, 355 (2000).

[22] Pushpendra P. Singh, B. P. Singh, Manoj Kumar Sharma, Unnati, Devendra P. Singh, R. Prasad, Rakesh Kumar, and K. S. Golda, Phys. Rev. C **77**, 014607 (2008).

[23] H. Morgenstern, W. Bohne, W. Galster, K. Grabisch, and A. Kyanowski, Phys. Rev. Lett. **52**, 1104 (1984).

[24] M. F. Vineyard, J. S. Bauer, J. F. Crum, C. H. Gosdin, R. S. Trotter, D. G. Kovar, C. Beck, D. J. Henderson, R. V. F. Janssens, B. D. Wilkins, C. F. Maguire, J. F. Mateja, F. W. Prosser, and G. S. F. Stephans, Phys. Rev. C **45**, 1784 (1992).

[25] R. Wada *et al.*, Phys. Rev. C **39**, 497 (1989).

[26] A. Chbihi, L. G. Sobotka, Z. Majka, D. G. Sarantites, D. W. Stracener, V. Abenante, T. M. Semkow, N. G. Nicolis, D. C. Hensley, J. R. Beene, and M. L. Halbert, Phys. Rev. C **43**, 652 (1991).

[27] P. Piattelli *et al.*, Phys. Lett. B **442**, 48 (1998).

[28] K. Yoshida, J. Kasagi, H. Hama, M. Sakurai, M. Kodama, K. Furutaka, K. Ieki, W. Galster, T. Kubo, M. Ishihara, and A. Galonsky, Phys. Rev. C **46**, 961 (1992).

[29] R. J. Charity, Phys. Rev. C **82**, 014610 (2010).

[30] A. Bonasera, R. Coniglione, and P. Sapienza, Eur. Phys. J. A **30**, 47 (2006), and references therein.

[31] H. Fuchs and K. Mohring, Rep. Prog. Phys. **57**, 231 (1994).

[32] R. Alba, R. Coniglione, A. Del Zoppo, C. Agodi, G. Bellia, P. Finocchiaro, K. Loukachine, C. Maiolino, E. Migneco, P. Piattelli, D. Santonocito, P. Sapienza, A. Peghaire, I. Iori, L. Manduci, and A. Moroni, Phys. Lett. B **322**, 38 (1994).

[33] P. Pawlowski *et al.*, Eur. Phys. J. A **9**, 371 (2000).

[34] V. Avdeichinov, R. Ghetti, J. Helgesson, B. Jakobsson, P. Golubev, N. Colonna, and H. W. Wilschut, Nucl. Phys. A **736**, 22 (2004).

[35] P. Sapienza *et al.*, Phys. Rev. Lett. **87**, 072701 (2001).

[36] M. P. Kelly, K. A. Snover, J. P. S. van Schagen, M. Kicińska-Habior, and Z. Trznadel, Phys. Rev. Lett. **82**, 3404 (1999).

[37] W. Cassing, V. Metag, U. Mosel, and K. Niita, Phys. Rep. **188**, 363 (1990).

[38] Y. Schutz *et al.*, Nucl. Phys. A **622**, 404 (1997).

[39] H. Nifenecker and J. A. Pinston, Annu. Rev. Nucl. Part. Sci. **40**, 113 (1990).

[40] F. Pulhofer, Nucl. Phys. A **280**, 267 (1977).

[41] I. Dioszegi, Phys. Rev. C **64**, 019801 (2001), and reference therein.

[42] D. R. Chakrabarty, S. Sen, M. Thoennessen, N. Alamanos, P. Paul, R. Schicker, J. Stachel, and J. J. Gaardhøje, Phys. Rev. C **36**, 1886 (1987).

[43] J. B. Natowitz, R. Wada, K. Hagel, T. Keutgen, M. Murray, A. Makeev, L. Qin, P. Smith, and C. Hamilton, Phys. Rev. C **65**, 034618 (2002), and references therein.

[44] W. E. Ormand, P. F. Bortignon, A. Bracco, and R. A. Broglia, Phys. Rev. C **40**, 1510 (1989).

[45] A. V. Ignatyuk, G. N. Smirenin, and A. S. Tishin, Sov. J. Nucl. Phys. **21**, 255 (1975).

[46] W. Reisdorf, Z. Phys. A: At. Nucl. **300**, 227 (1981).

[47] G. Bellia, R. Alba, R. Coniglione, A. Del Zoppo, P. Finocchiaro, C. Maiolino, E. Migneco, P. Piattelli, P. Sapienza, N. Frascaria, I. Lhenry, J. C. Roynette, T. Suomijärvi, N. Alamanos, F. Auger, A. Gillibert, D. Pierroutsakou, J. L. Sida, and P. R. Silveira Gomes, Nucl. Instrum. Methods Phys. Res., Sect. A **329**, 173 (1993).

[48] J. P. Lestone, Phys. Rev. C **52**, 1118 (1995).

[49] S. Shlomo and J. B. Natowitz, Phys. Rev. C **44**, 2878 (1991).

[50] B. Martin *et al.*, Phys. Lett. B **664**, 47 (2008).

[51] D. Pierroutsakou *et al.*, Phys. Rev. C **80**, 024612 (2009).

[52] H. Nifenecker, J. Blachot, J. Crancon, A. Gizon, and A. Lleres, Nucl. Phys. A **447**, 533 (1986).

[53] J. Pochodzalla *et al.*, Phys. Rev. Lett. **75**, 1040 (1995).

[54] Y. G. Ma, Eur. Phys. J. A **30**, 227 (2006), and references therein.

[55] B. Borderie and P. Desesquelles, Eur. Phys. J. A **30**, 243 (2006), and references therein.

[56] F. Gulminelli and M. D'Agostino, Eur. Phys. J. A **30**, 253 (2006), and references therein.

[57] O. Lopez and M. F. Rivet, Eur. Phys. J. A **30**, 263 (2006), and references therein.

[58] P. Chomaz, M. Di Toro, and A. Smerzi, Nucl. Phys. A **563**, 509 (1993).

[59] A. Bonasera, M. Bruno, C. A. Dorso, and P. F. Mastinu, Riv. Nuovo Cimento **23**, 1 (2000).

[60] S. Tudisco, G. Cardella, F. Amorini, A. Anzalone, A. Di Pietro, P. Figuera, F. Giustolisi, G. Lanzalone, Lu Jun, A. Musumarra, M. Papa, S. Pirrone, and F. Rizzo, Europhys. Lett. **58**, 811 (2002).

[61] F. Amorini, G. Cardella, A. Di Pietro, P. Figuera, G. Lanzalone, Lu Jun, A. Musumarra, M. Papa, S. Pirrone, F. Rizzo, W. Tian, and S. Tudisco, Phys. Rev. C **69**, 014608 (2004).